Progressive amorphization of GeSbTe phase-change material under electron beam irradiation

Cite as: APL Mater. **7**, 081121 (2019); https://doi.org/10.1063/1.5102075 Submitted: 23 April 2019 . Accepted: 08 August 2019 . Published Online: 27 August 2019

Ting-Ting Jiang, Jiang-Jing Wang (10), Lu Lu, Chuan-Sheng Ma, Dan-Li Zhang, Feng Rao (10), Chun-Lin Jia, and Wei Zhang (10)

COLLECTIONS

Paper published as part of the special topic on Emerging Materials in Neuromorphic Computing
Note: Note: This paper is part of the special topic on Emerging Materials in Neuromorphic Computing.









ARTICLES YOU MAY BE INTERESTED IN

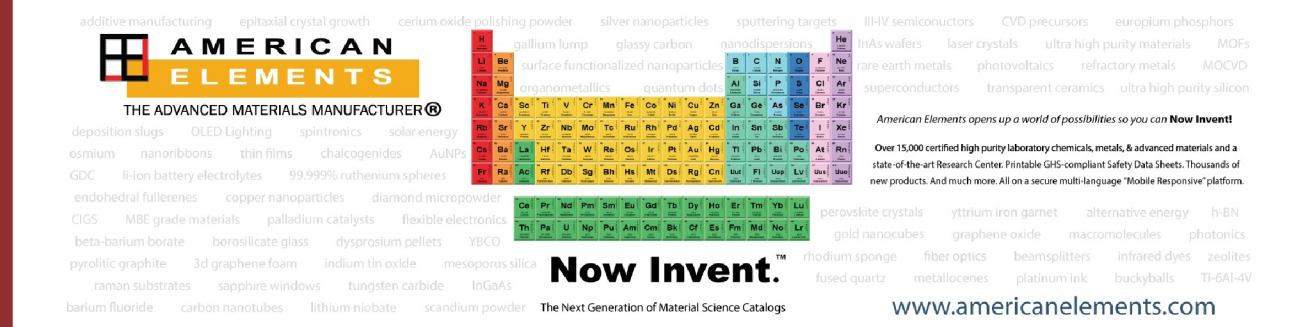
Multilevel HfO₂-based RRAM devices for low-power neuromorphic networks APL Materials **7**, 081120 (2019); https://doi.org/10.1063/1.5108650

Behavioral modeling of integrated phase-change photonic devices for neuromorphic computing applications

APL Materials 7, 091113 (2019); https://doi.org/10.1063/1.5111840

Ferroelectric materials for neuromorphic computing APL Materials 7, 091109 (2019); https://doi.org/10.1063/1.5108562





Progressive amorphization of GeSbTe phase-change material under electron beam irradiation

Cite as: APL Mater. 7, 081121 (2019); doi: 10.1063/1.5102075 Submitted: 23 April 2019 • Accepted: 8 August 2019 •

Published Online: 27 August 2019







Ting-Ting Jiang,¹ Jiang-Jing Wang,^{1,2,a)} Lu Lu,³ Chuan-Sheng Ma,³ Dan-Li Zhang,¹ Feng Rao,⁴ Chun-Lin Jia,^{3,5} and Wei Zhang^{1,a)}

AFFILIATIONS

- ¹Center for Advancing Materials Performance from the Nanoscale, State Key Laboratory for Mechanical Behavior of Materials, Xi'an Jiaotong University, Xi'an 710049, China
- ²The School of Chemistry and Chemical Engineering, Yulin University, Yulin 719000, China
- The School of Microelectronics, State Key Laboratory for Mechanical Behavior of Materials, Xi'an Jiaotong University, Xi'an 710049, China
- College of Materials Science and Engineering, Shenzhen University, Shenzhen 518060, China
- ⁵Ernst Ruska-Centre for Microscopy and Spectroscopy with Electrons, Forschungszentrum Jülich GmbH, 52425 Jülich, Germany

Note: This paper is part of the special topic on Emerging Materials in Neuromorphic Computing.

^{a)} Authors to whom correspondence should be addressed: wangjiangjing@stu.xjtu.edu.cn and wzhang0@mail.xjtu.edu.cn

ABSTRACT

Fast and reversible phase transitions in chalcogenide phase-change materials (PCMs), in particular, Ge-Sb-Te compounds, are not only of fundamental interests but also make PCMs based random access memory a leading candidate for nonvolatile memory and neuromorphic computing devices. To RESET the memory cell, crystalline Ge-Sb-Te has to undergo phase transitions first to a liquid state and then to an amorphous state, corresponding to an abrupt change in electrical resistance. In this work, we demonstrate a progressive amorphization process in GeSb₂Te₄ thin films under electron beam irradiation on a transmission electron microscope (TEM). Melting is shown to be completely absent by the *in situ* TEM experiments. The progressive amorphization process resembles closely the cumulative crystallization process that accompanies a continuous change in electrical resistance. Our work suggests that if displacement forces can be implemented properly, it should be possible to emulate symmetric neuronal dynamics by using PCMs.

© 2019 Author(s). All article content, except where otherwise noted, is licensed under a Creative Commons Attribution (CC BY) license (http://creativecommons.org/licenses/by/4.0/). https://doi.org/10.1063/1.5102075

Artificial intelligence, big data analytics, and other data-intensive applications are changing our lives rapidly and profoundly. They, however, also pose a significant challenge to data storage and processing to the current computing architecture, which physically separates storage units from processing units. The extensive data shuffling between these units over bandwidth limited interconnects leads to a fundamental barrier in improving the computing efficiency. The emerging neuromorphic computing devices ^{1–7} hold the promise to break this barrier by unifying storage with processing in a single cell. Phase change materials (PCMs) based random access memory (PRAM) is one of the leading candidates for this application. ^{6–14}

PRAM is technologically mature and has entered the global memory market as Storage-Class Memory (SCM) recently, ¹⁵ filling the performance gap between dynamic random access memory (DRAM) and flash memory based solid state hard drive (SSD). The basic principle of PRAM is to exploit the large contrast in electrical resistance, and the rapid and reversible transitions between two solid states of PCMs, i.e., a disordered amorphous state and an ordered crystalline state. ¹⁶ Among the explored PCMs, Ge-Sb-Te compounds along the GeTe-Sb₂Te₃ pseudobinary line, ^{17–25} such as Ge₂Sb₂Te₅ and GeSb₂Te₄, are the most widely studied materials. Upon crystallization, amorphous (amor-) Ge-Sb-Te compounds form a metastable cubic rocksalt (cub-) phase.

One key attribute of PCM for neuromorphic computing is that its crystallization process can be accomplished by multiple narrow voltage pulses in a cumulative mode, corresponding to a partial SET process of PRAM.⁷ The change in electrical conductance of the memory cell is then dependent on the previous excitation. This history-dependent behavior of electrical resistance classifies PRAM as memristors. ^{36,37} To RESET the crystallized PRAM cell, a high voltage pulse is applied to melt down the crystalline state, and the amorphous state is obtained upon rapid cooling. This melt-quench procedure leads to an abrupt RESET process, hindering the emulation of symmetric neuronal dynamics using PCMs.⁷

Here, we demonstrate a progressive amorphization process in GeSb₂Te₄ (short as GST in the following) thin films under electron beam (E-beam) irradiation on a transmission electron microscope (TEM). TEM is an important technique to assess the microstructure and elemental distribution of materials, while as high energy particle beams, electron beams can also be used to cause temporary or permanent changes of the specimen structure, e.g., to induce phase transitions of PCMs. In this work, *in situ* E-beam irradiation experiments were performed on a JEOL JEM-2100F TEM under 200 keV and a FEI Titan G2 aberration-corrected TEM under 300 keV.

GST films of ~80 nm-thick were deposited with magnetron sputtering on ultrathin carbon film (~5 nm) TEM grids and were covered by an electron-transparent ZnS-SiO₂ layer to prevent oxidization. The GST thin films were in the amorphous phase upon sputtering. One set of samples was irradiated using electron beams, while another set of samples was annealed at 150 °C for 1 h in argon atmosphere (flow rates of 1200 sccm) in a regular tube furnace for comparison. The thermal-based and E-beam-based phase transitions of GST are depicted in Fig. 1. Upon heating, the amorphase crystallizes into the cub-phase at ~150 °C, while to induce the reversed transition, the cub-phase needs to be melted at ~650 °C and then rapidly cooled down to room temperature. In contrast, direct and reversible phase transitions between amor-GST and cub-GST can be obtained by manipulating the beam intensity, accelerating voltage, and irradiation time of TEM.

We start our irradiation experiment on the JEOL JEM-2100F TEM with a fixed accelerating voltage of 200 keV and a set beam intensity of $6.0 \times 10^{23} \ e \ m^{-2} \ s^{-1}$ (dose, $5.4 \times 10^8 \ e \ nm^{-2}$). The amorphous nature of the initial phase is confirmed by the halo rings of the

selected area electron diffraction (SAED) patterns [Fig. 2(a)]. Multiple crystal nuclei appear after 5 min irradiation, leading to visible changes in contrast of the bright-field image and diffraction rings in the SAED pattern [Fig. 2(b)]. Upon further irradiation to 15 min, randomly oriented crystal grains with average size of 10-20 nm are observed, and the corresponding SAED pattern shows bright and sharp diffraction rings with cub-phase characteristics [Fig. 2(c)], which are comparable with those of the thermally annealed sample [Fig. 2(f)]. This E-beam-induced crystallization has been observed consistently in PCMs.³⁸⁻⁴¹ By reducing the beam intensity, crystallization was effectively prohibited. For example, no obvious change in amorphous GST could be observed in JEOL JEM-2100F TEM with beam intensity lower than 1.6×10^{23} e m⁻² s⁻¹ within 90 min⁴¹ (this beam intensity value at irradiation area corresponds to the value of 1.0×10^{12} e m⁻² s⁻¹ at screen shown in Ref. 41). Such time window is sufficiently long for TEM measurements to assess the structural details amorphous GST.4

It was concluded that in addition to heating effects, the displacement damage by knock-on collisions of E-beams⁴³ also plays a role in triggering crystallization in GST thin films. 38 Significant atomic displacement was also observed in crystalline GST by focusing the electron beam to a small area for extensive irradiation. 44,45 Following the same strategy, we made the electron beams more focused to increase the probability of knock-on collisions and to check if this kinetic effect could be strong enough to induce amorphization like the case of ion beam irradiations. 46,47 Indeed, parts of the irradiation-crystallized thin film transformed into the amorphous phase [Fig. 2(d)] after 45 min E-beam irradiation, and after 75 min, almost all the cubic grains vanished and dim halo rings appeared in the SAED pattern [Fig. 2(e)]. The measured beam intensity was $1.1\times10^{24}~e~m^{-2}~s^{-1}$ (dose, $4.95\times10^9~e~nm^{-2}$). The same irradiation experiment was also carried out on the thermally annealed cubic-phase sample, and a similar amorphization process was observed over ~80 min. No sign of amorphization can be observed, if the electron beams are less focused (beam intensity below $\sim 8.0 \times 10^{23} \ e \ m^{-2} \ s^{-1}$). The irradiation-induced amorphous GST can be further crystallized upon electron beam

It is noted that the observed irradiation-induced amorphization process is continuous and no abrupt change in structural

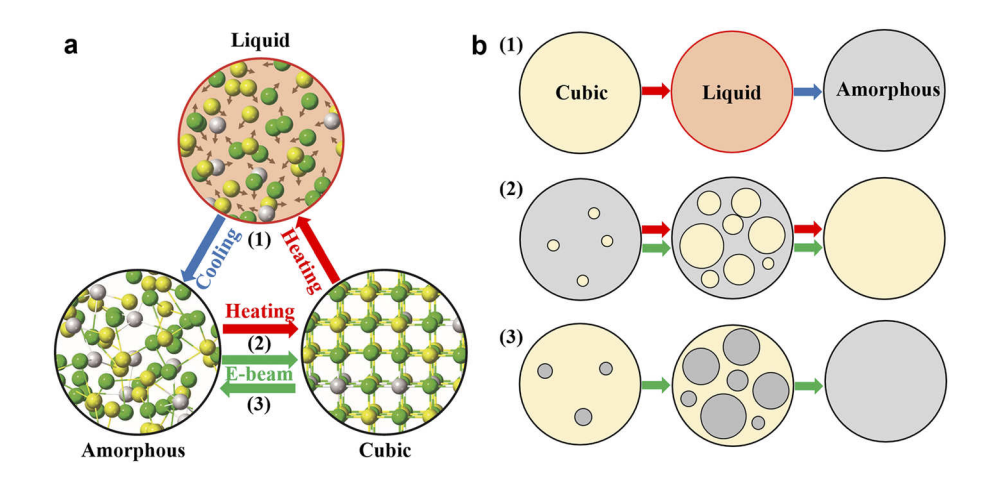


FIG. 1. Phase transition paths of GST. (a) Crystallization can be accomplished by heating, while to trigger amorphization by thermal power, melting and subsequent rapid cooling are necessary. As regards electron beam (E-beam) irradiation, direct and reversible solid-state transitions can be achieved. (b) The sketches of (1) abrupt amorphization by melt-quenching, (2) progressive crystallization upon heating or by E-beam irradiation, and (3) progressive amorphization by E-beam irradiation.

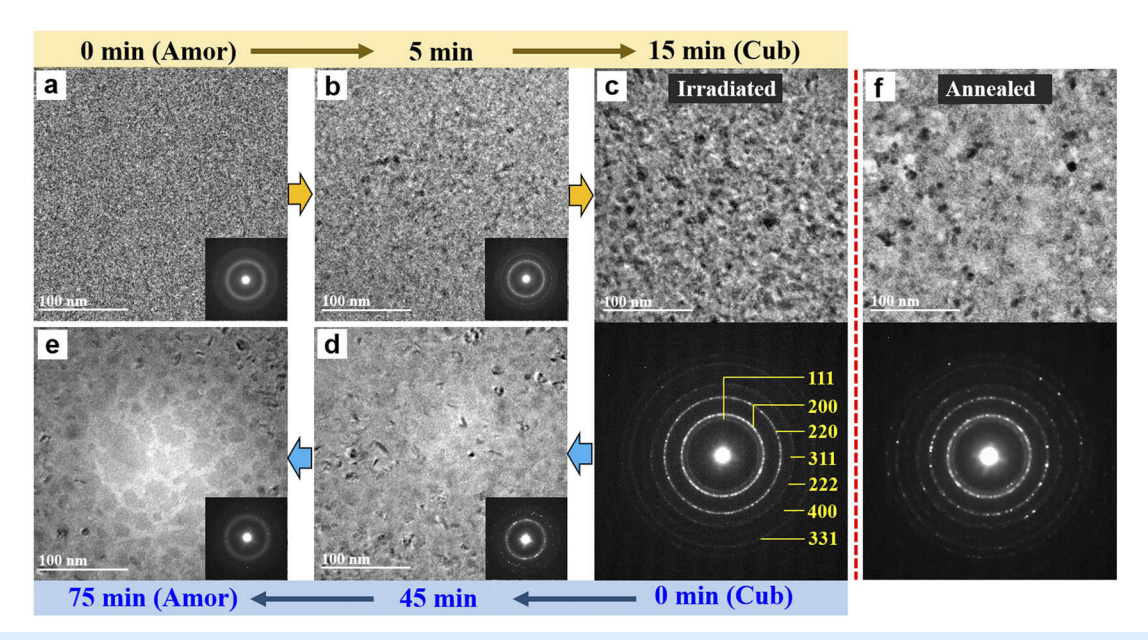


FIG. 2. The bright-field TEM images and the corresponding SAED patterns of GST, recorded under electron beam irradiation. [(a)–(c)] Crystallization. [(c)–(e)] Amorphization. The critical parameter in inducing the opposite transitions is beam intensity, i.e., 6.0×10^{23} e m⁻² s⁻¹ (dose, 5.4×10^{8} e nm⁻²) for crystallization and 1.1×10^{24} e m⁻² s⁻¹ (dose, 4.95×10^{9} e nm⁻²) for amorphization. The accelerating voltage is the same, 200 keV. (f) TEM image and the corresponding SAED pattern of GST thin films annealed at 150 °C for 1 h, showing the comparable features of the E-beam induced cubic GST sample shown in (c).

patterns could be observed, which indicates a nonthermal phase transition to the amorphous state, bypassing the melt-quench process. To gain additional support of a nonthermal-dominated transition, we made a rough estimate of the temperature increase in

the thin film of GST following the equation 48 $\Delta T = \frac{I}{\pi ke} \left(\frac{\Delta E}{d}\right) \ln \frac{b}{r_0}$ in which e, I, r_0 , k, and b are the electron's charge, beam current, beam radius, thermal conductivity, and sample radius, respectively. ΔE is the total energy loss per electron in a sample of thickness d.

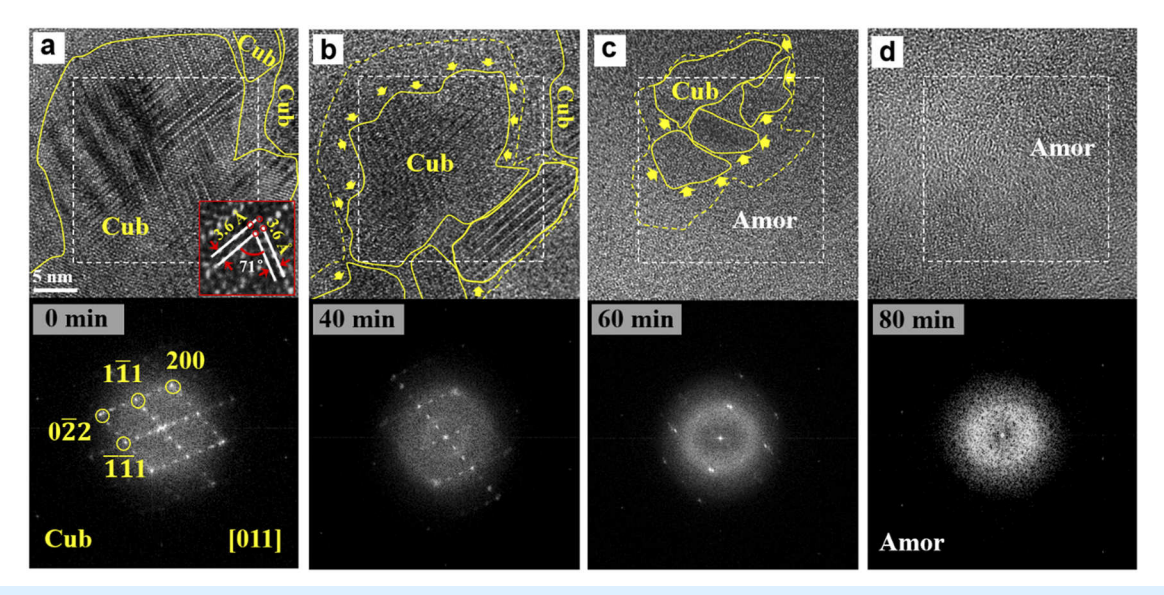


FIG. 3. In situ amorphization of cubic GST under 200 keV E-beam irradiation. [(a)–(d)] The snapshots of phase transition from the cub-phase to amor-phase as a function of irradiation time, showing the stages for separation and shrinking of the cub-phase grains. After 80 min irradiation, all the cub-phase grains turn amorphous completely. The image areas in the dashed white boxes in the bright-field images are used for the calculations of fast Fourier transform (FFT) patterns.

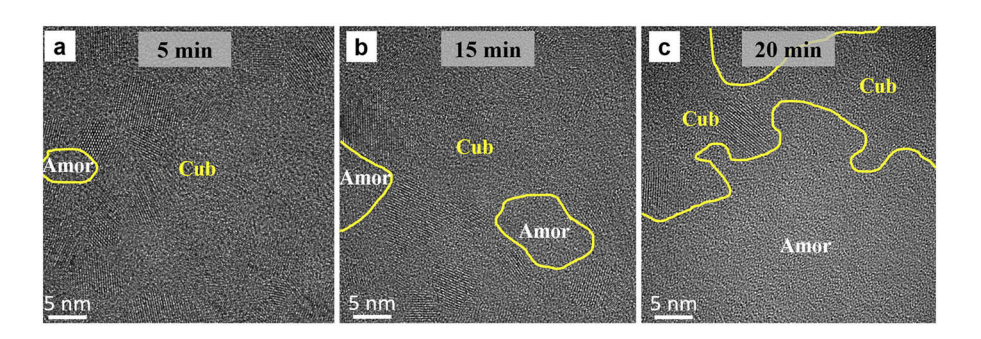


FIG. 4. *In situ* amorphization of cub-GeSb₂Te₄ under 300 keV e-beam irradiation with a beam intensity $\sim 1.9 \times 10^{32}$ e m⁻² s⁻¹ (dose, $\sim 2.28 \times 10^{17}$ e nm⁻²). [(a)–(c)] The snapshots of phase transition from the cub-phase to amor-phase as a function of irradiation time. Higher accelerating voltage and higher beam intensity lead to a more rapid amorphization process.

The estimated maximum temperature rise is ~220 $^{\circ}$ C, which is well below the melting point of GST (~650 $^{\circ}$ C). In fact, GST thin films will evaporate quickly above 450 $^{\circ}$ C, and it is not feasible to observe the melting process at ~650 $^{\circ}$ C in unencapsulated GST thin films

To explore the structural details during the E-beam induced amorphization process, high resolution TEM (HRTEM) characterizations were carried out. Figure 3(a) shows the initial stage. The center target grain shows [011]-orientation of cubic lattice, as evidenced by its fast Fourier transform (FFT) pattern. The FFT pattern corresponds to the white dashed box in the HRTEM image. The inset depicts a zoomed-in view of the area inside the red box, showing that the interplane spacing of (111) is 3.6 Å and the angle between (1 $\bar{1}1$) and (111) is 71°. Upon E-beam irradiation over 40 min [Fig. 3(b)], the original [011]-oriented grain (marked by a dashed yellow line) split into four cub-phase grains with different orientations. The orientation of the primary grain [solid lines in Fig. 3(b)] remained unchanged. At this stage, amorphization also took place, which reduced the size of the primary grain, as indicated by arrows in Fig. 3(b). Another 20 min irradiation amorphized the major parts of the irradiation area, and the initial grain further split into several smaller parts [Fig. 3(c)]. Finally, all the cub-phase grains disappeared and the whole irradiation area turned amorphous after 80 min irradiation, as confirmed by the corresponding FFT pattern

This direct cub- to amor-GST transition path under E-beam irradiation is in a stark contrast with the conventional transition path induced by thermal melt-quenching. Clearly, no abrupt structural change to the liquid state could be observed during the *in situ* TEM experiments. Instead, the E-beam induced amorphization undergoes gradual structural rearrangement locally, which can be attributed to the knock-on effects of E-beams. In general, for electron illumination of thin specimen, a higher accelerating voltage results in less effects of specimen heating, but stronger kinetic effects of knock-on collisions. 49,50 For further confirmation, we performed in situ experiments on a FEI Titan G2 TEM operated at 300 keV. It was found that the beam intensity in this TEM can reach ~1.9 $\times 10^{32} e \text{ m}^{-2} \text{ s}^{-1} \text{ (dose, } \sim 2.28 \times 10^{17} e \text{ nm}^{-2} \text{)}$. Starting from cub-GST, amorphization already proceeded after 5 min irradiation, as shown in Fig. 4(a). As the irradiation time increased, the amorphous region expanded gradually and rapidly [Figs. 4(b) and 4(c)]. The faster amorphization on the FEI Titan G2 TEM than on the JEOL JEM-2100F TEM can be understood due to the irradiation by the beam with much higher intensity and at the higher accelerating voltage. As stated above, the knock-on collision effects should be the major source for amorphization, as heating effects should easily evaporate the unencapsulated thin film.

In summary, we have demonstrated an effective approach to achieve reversible and direct crystallization and amorphization of GeSb₂Te₄ in a progressive manner by means of E-beam irradiation. The chief TEM parameters for these transitions are found to be accelerating voltage, beam intensity, and irradiation time. The in situ irradiation experiments provide a real-time and real-space view of progressive structural evolution between the two solid state phases, where melting is completely absent. The knock-on collision effect of E-beams drives this nonthermal amorphization process. We note that the displacement forces induced by electron or ion beam irradiations are not likely to be implemented in electronic devices, while mechanical forces and strains induced by, e.g., piezoelectric materials⁵¹ appear to be a more suitable approach.⁵ A previous work on a silicon nanopillar also shows a continuous and progressive nonthermal amorphization process under uniaxial strain.⁵³ Similar experiments are anticipated to be carried out in PCMs. If displacement forces can be properly implemented, symmetric neuronal dynamics could possibly be emulated using

W.Z. is thankful for the support from the National Natural Science Foundation of China (Grant No. 61774123), 111 Project 2.0 (Grant No. BP2018008), the Science and Technology Department of Jiangsu Province (No. BK20170414), and the Young Talent Support Plan of Xi'an Jiaotong University. F.R. gratefully acknowledges the National Natural Science Foundation of China (Grant No. 61622408), the Major Provincial Basic Research Program of Guangdong (Grant No. 2017KZDXM070), and the Science and Technology Foundation of Shenzhen (Grant No. JCYJ20180507182248605). The authors also acknowledge the support from the International Joint Laboratory for Micro/Nano Manufacturing and Measurement Technologies of Xi'an Jiaotong University.

REFERENCES

¹Q. Xia and J. J. Yang, Nat. Mater. 18, 309 (2019).

²M. A. Zidan, J. P. Strachan, and W. D. Lu, Nat. Electron. 1, 22 (2018).

³Y. Yang and R. Huang, Nat. Electron. 1, 274 (2018).

⁴D. Ielmini and H.-S. P. Wong, Nat. Electron. 1, 333 (2018).

⁵M. Wang, S. Cai, C. Pan, C. Wang, X. Lian, Y. Zhuo, K. Xu, T. Cao, X. Pan, B. Wang, S.-J. Liang, J. J. Yang, P. Wang, and F. Miao, Nat. Electron. 1, 130 (2018).

⁶W. Zhang, R. Mazzarello, M. Wuttig, and E. Ma, Nat. Rev. Mater. **4**, 150 (2019).

- ⁷A. Sebastian, M. Le Gallo, G. W. Burr, S. Kim, M. BrightSky, and E. Eleftheriou, J. Appl. Phys. **124**, 111101 (2018).
- ⁸ M. Le Gallo, A. Sebastian, R. Mathis, M. Manica, H. Giefers, T. Tuma, C. Bekas, A. Curioni, and E. Eleftheriou, Nat. Electron. 1, 246 (2018).
- ⁹S. Ambrogio, P. Narayanan, H. Tsai, R. M. Shelby, I. Boybat, and G. W. Burr, Nature 558, 60 (2018).
- ¹⁰C. Ríos, N. Youngblood, Z. Cheng, M. L. Gallo, W. H. P. Pernice, C. D. Wright, A. Sebastian, and H. Bhaskaran, Sci. Adv. 5, eaau5759 (2019).
- ¹¹Z. Cheng, C. Ríos, W. H. P. Pernice, C. D. Wright, and H. Bhaskaran, Sci. Adv. 3, e1700160 (2017).
- ¹²I. Boybat, M. Le Gallo, S. R. Nandakumar, T. Moraitis, T. Parnell, T. Tuma, B. Rajendran, Y. Leblebici, A. Sebastian, and E. Eleftheriou, Nat. Commun. 9, 2514 (2018)
- ¹³T. Tuma, A. Pantazi, M. Le Gallo, A. Sebastian, and E. Eleftheriou, Nat. Nanotechnol. 11, 693 (2016).
- ¹⁴C. D. Wright, Y. Liu, K. I. Kohary, M. M. Aziz, and R. J. Hicken, Adv. Mater. 23, 3408 (2011).
- ¹⁵S. W. Fong, C. M. Neumann, and H.-S. P. Wong, IEEE Trans. Electron Devices 64, 4374 (2017).
- ¹⁶M. Wuttig and N. Yamada, Nat. Mater. 6, 824 (2007).
- ¹⁷N. Yamada, E. Ohno, K. Nishiuchi, N. Akahira, and M. Takao, J. Appl. Phys. **69**, 2849 (1991).
- ¹⁸N. Yamada and T. Matsunaga, J. Appl. Phys. **88**, 7020 (2000).
- ¹⁹Z. Sun, J. Zhou, and R. Ahuja, Phys. Rev. Lett. **96**, 055507 (2006).
- ²⁰ A. V. Kolobov, P. Fons, A. I. Frenkel, A. L. Ankudinov, J. Tominaga, and T. Uruga, Nat. Mater. 3, 703 (2004).
- ²¹ M. Xu, Y. Cheng, H. Sheng, and E. Ma, Phys. Rev. Lett. **103**, 195502 (2009).
- ²² W. Zhang, A. Thiess, P. Zalden, R. Zeller, P. H. Dederichs, J. Y. Raty, M. Wuttig, S. Blügel, and R. Mazzarello, Nat. Mater. 11, 952 (2012).
- ²³ J.-J. Wang, J. Wang, H. Du, L. Lu, P. C. Schmitz, J. Reindl, A. M. Mio, C.-L. Jia, E. Ma, R. Mazzarello, M. Wuttig, and W. Zhang, Chem. Mater. 30, 4770 (2018).
- ²⁴J.-J. Wang, Y.-Z. Xu, R. Mazzarello, M. Wuttig, and W. Zhang, Materials 10, 862 (2017).
- ²⁵ J. Orava, A. L. Greer, B. Gholipour, D. W. Hewak, and C. E. Smith, Nat. Mater. 11, 279 (2012).
- ²⁶N. Yamada, MRS Bull. **21**, 48 (1996).
- ²⁷B. J. Kooi and J. T. M. De Hosson, J. Appl. Phys. **92**, 3584 (2002).
- ²⁸T. Matsunaga and N. Yamada, Phys. Rev. B **69**, 104111 (2004).
- ²⁹ U. Ross, A. Lotnyk, E. Thelander, and B. Rauschenbach, Appl. Phys. Lett. 104, 121904 (2014).

- ³⁰B. Zhang, W. Zhang, Z.-J. Shen, Y.-J. Chen, J.-X. Li, S.-B. Zhang, Z. Zhang, M. Wuttig, R. Mazzarello, E. Ma, and X.-D. Han, Appl. Phys. Lett. **108**, 191902 (2016).
- 31 A. Lotnyk, S. Bernütz, X. Sun, U. Ross, M. Ehrhardt, and B. Rauschenbach, Acta Mater. 105, 1 (2016).
- ³²Y. Zheng, M. Xia, Y. Cheng, F. Rao, K. Ding, W. Liu, Y. Jia, Z. Song, and S. Feng, Nano Res. 9, 3453 (2016).
- ³³Y. Zheng, Y. Wang, T. Xin, Y. Cheng, R. Huang, P. Liu, M. Luo, Z. Zhang, S. Lv, Z. Song, and S. Feng, Commun. Chem. 2, 13 (2019).
- ³⁴ M. Zhu, K. Ren, L. Liu, S. Lv, X. Miao, M. Xu, and Z. Song, Phys. Rev. Mater. 3, 033603 (2019).
- ³⁵M. Behrens, A. Lotnyk, J. W. Gerlach, I. Hilmi, T. Abel, P. Lorenz, and B. Rauschenbach, Nanoscale 10, 22946 (2018).
- ³⁶L. O. Chua, Nat. Electron. 1, 322 (2018).
- ³⁷C. D. Wright, L. Wang, M. M. Aziz, J. A. V. Diosdado, and P. Ashwin, Phys. Status Solidi B 249, 1978 (2012).
- ³⁸B. J. Kooi, J. Appl. Phys. **95**, 924 (2004).
- ³⁹ R. Pandian, B. J. Kooi, J. T. M. D. Hosson, and A. Pauza, J. Appl. Phys. **101**, 053529 (2007).
- ⁴⁰J. Tomforde, W. Bensch, L. Kienle, V. Duppel, P. Merkelbach, and M. Wuttig, Chem. Mater. 23, 3871 (2011).
- ⁴¹ J.-J. Wang, T.-T. Jiang, L. Tian, D.-L. Zhang, and W. Zhang, Mater. China 38, 110 (2019).
- ⁴² A. Hirata, T. Ichitsubo, P. F. Guan, T. Fujita, and M. W. Chen, Phys. Rev. Lett. 120, 205502 (2018).
- ⁴³N. Jiang and J. C. H. Spence, Ultramicroscopy 113, 77 (2012).
- ⁴⁴ A. Lotnyk, U. Ross, T. Dankwort, I. Hilmi, L. Kienle, and B. Rauschenbach, Acta Mater. 141, 92 (2017).
- ⁴⁵ A. Lotnyk, T. Dankwort, I. Hilmi, L. Kienleb, and B. Rauschenbacha, Nanoscale 11, 10838 (2019).
- ⁴⁶S. M. S. Privitera, A. M. Mio, E. Smecca, A. Alberti, W. Zhang, R. Mazzarello, J. Benke, C. Persch, F. La Via, and E. Rimini, Phys. Rev. B 94, 094103 (2016).
- ⁴⁷S. Privitera, A. M. Mio, W. Zhang, R. Mazzarello, C. Persch, M. Wuttig, and E. Rimini, Nanosci. Nanotechnol. Lett. 9, 1095 (2017).
- ⁴⁸X. Qu and Q. Deng, RSC Adv. 7, 37032 (2017).
- ⁴⁹ R. F. Egerton, Microsc. Res. Tech. **75**, 1550 (2012).
- ⁵⁰D. B. Williams and C. B. Carter, Transmission Electron Microscopy A Textbook for Material Science (Springer Press, New York, 2009).
- for Material Science (Springer Press, New York, 2009). ⁵¹Z. L. Wang and J. Song, Science **312**, 242 (2006).
- ⁵² J. Li, Z. Shan, and E. Ma, MRS Bull. **39**, 108 (2014).
- ⁵³Y. C. Wang, W. Zhang, L. Y. Wang, Z. Zhuang, E. Ma, J. Li, and Z. W. Shan, NPG Asia Mater. 8, e291 (2016).